

**Non-Potential Features Observed in the Magnetic Field
of an Active Region**

G. A. GARY, R. L. MOORE, AND M. J. HAGYARD
Space Science Laboratory
Marshall Space Flight Center
Huntsville, AL 35812 USA

BERNHARD M. HAISCH
Lockheed Palo Alto Research Laboratory
Palo Alto, CA 94304

Received _____

Running Title: Non-Potential Active Region

(NASA-TM-89383) NON-POTENTIAL FEATURES
OBSERVED IN THE MAGNETIC FIELD OF AN ACTIVE
REGION (NASA) 46 p Avail: NTIS

N87-70450

Unclas
00/46 0079432

T. I. S. LIBRARY

1986 JUN 18 PM 3:56

RECEIVED
JUN 17 1986

ABSTRACT

The observed vector magnetic field of an active region (NOAA AR 2684 on 23 September 1980) is analyzed for non-potential features. For this active region, there is a unique complementary set of observations especially well suited for study of the vector field: vector magnetograms from MSFC, Ly-alpha and 1600 Å UV continuum photographs from the LPSP/LPARL Transition Region Camera flown on a rocket, and H α filtergrams from the Herzberg Institute of Astrophysics and from the USAF Solar Optical Observing Network. The non-potential aspects of the magnetic field are brought out by comparing the observed photospheric vector field with observed chromospheric fibrils and with computed potential and linear force-free fields. The main findings are:

1. The overall bipolar magnetic field of the active region had a net twist corresponding to net current flowing anti-parallel to the field. The average density of this net current was of order 4×10^{-4} amp m $^{-2}$; the total net current was of order 3×10^{12} amp.

2. In the interior of the active region, there were three regions of enhanced non-potentiality. In one of these regions, differences in direction between the photospheric transverse field vector and the H-alpha fibrils, and between these and the Ly-alpha fibrils, showed that the field had a marked non-potential twist or shear with height above the photosphere.

3. At least two of the three local regions of enhanced non-potentiality were sites of flares that occurred within a few hours of the time of the field observations. One of the flare sites was the region of vertical magnetic shear.

4. The total non-potential magnetic energy stored in a global sense in the active region was measured to be of order 10^{32} erg, which was about 3σ above the noise level. This shows that the uncertainty in the vector field measurements must be substantially reduced in order to confidently measure the buildup and release of magnetic energy in any but the very largest flares.

Subject headings: Sun: magnetic fields--- Sun: flares---
Sun: chromosphere --- Sun: corona

Non-Potential Features Observed in the Magnetic Field of an Active Region

I. INTRODUCTION

It is now clear that the structure of an active region is determined largely, if not entirely, by the structure of the magnetic field and that the field topology above the photosphere is determined principally by the distribution of magnetic flux in the photosphere (c.f., Stenflo 1983; Priest 1982; Orrall 1981 for overviews). Although high resolution microwave interferometry is beginning to be used to observe magnetic structures high above the photosphere (i.e., in the corona), to interpret such observations in terms of coronal magnetic field strengths and topology it is still necessary to assume a model for the coronal field and plasma (c.f., Holman and Kundu 1985). In comparison, methods for determining the photospheric magnetic structure are well established (Harvey 1977). These methods depend on measurements of the Zeeman effect in photospheric spectral lines. While lines formed at different heights in the lower solar atmosphere have been used to infer the three-dimensional structure of magnetic fields (Giovannelli and Jones 1982; Kotov 1971), the range of heights is quite small (<1000 km) compared to the height reached by the magnetic field lines (c.f., x-ray images). To infer the large scale three-dimensional structure at greater heights, it is necessary to extrapolate from the magnetic field distribution in the photosphere; this is done using mathematical methods to solve the magnetostatic problem of

determining the magnetic field as a function of (1) observed boundary conditions on the surface (the photosphere) and (2) some assumed distribution of electric currents above the photosphere. The constructed three-dimensional magnetic field line model may then be compared with field line "tracers", like fibrils and loops observed in the chromosphere and corona of active regions.

Excellent summaries of methods to extrapolate solar magnetic field lines from photospheric magnetograms and suggested prescriptions for comparing such models to observations are given by Levine (1975,1976). If all of the currents giving rise to the magnetic field are subphotospheric, the field in the photosphere and above is a potential field, the state of minimum magnetic energy. Its three-dimensional structure is uniquely determined by the photospheric distribution of either B_l , the longitudinal component, or B_t , the transverse component (Schmidt 1964; Sakurai 1982; Hannakam, Gary and Teuber 1984). If there are electric currents in the photosphere and above and if the current \vec{J} is everywhere parallel to \vec{B} , the magnetic field, the configuration is called "force-free" since $\vec{J} \times \vec{B} = 0$; in this situation $\nabla \times \vec{B} = \mu_0 \vec{J} = \alpha \vec{B}$, where α is a scalar and $\mu_0 = 4\pi \times 10^{-3}$ G m amp⁻¹. Except in dynamic events, i.e. flares, the field should be very nearly force-free above the photosphere in active regions because the magnetic pressure greatly exceeds the gas pressure. If α is constant independent of the spatial coordinates, then once again B_l and/or B_t on the photosphere determines the three-dimensional structure of the magnetic field for a given α ,

(Nakagawa and Raadu 1972; Chiu and Hilton 1977; Alissandrakis 1981; Hannakam, Gary and Teuber 1984). In all likelihood α is not a constant everywhere within an active region. Methods are now being developed to calculate non-constant alpha solutions (Sakurai 1979, Sakurai 1981, Pridmore-Brown 1981, and Wu 1984), but are not yet a proven tool for the solar physicist.

It is now possible to measure all three components of the photospheric magnetic vector field; a vector magnetograph is in operation at the NASA Marshall Space Flight Center (MSFC; Hagyard et al. 1982; Hagyard, Low and Tandberg-Hanssen 1982). From the longitudinal component of the observed vector field, three-dimensional fields can be computed and compared with fieldline tracers above the photosphere. In addition, the computed transverse field in the photosphere can be directly compared with the observed transverse field. Potential and force-free models with such comparisons show where in the active region and to what degree the observed field is non-potential. Alternatively, the observed transverse field can be analyzed directly for the presence of currents entering or leaving the photosphere (Haisch et al. 1986, deLoach et al. 1984). In this paper, we use the comparison method; we examine the non-potentiality of a particular active region by comparing the observed photospheric transverse field and observed chromospheric field tracers with potential and linear force-free fields computed from the observed longitudinal field. The effect of the net total current is investigated. Hence, the large-scale (global) structure of the magnetic field is investigated instead of the 'fine' scale structure at the resolution limit of the observations.

Empirically, the magnetic field configurations of active regions can be classified into three general categories: (1) a simple bipolar magnetic structure closely satisfying a potential configuration and having no recent flaring history; (2) a complex (more than two polarity concentrations), non-potential configuration showing magnetic shear and having an active flare history (Hagyard et al. 1984); and (3) an intermediate case which may have a complex polarity structure and a flare history, but which has a largely potential magnetic field configuration. This study concerns itself with such an intermediate case: active region NOAA AR 2684 (Hale 17145) on 23 September 1980.

The active region AR 2684 appeared on the east limb on 17 September as a small growing bipolar region. When it was near disk center on the 23rd, the region obtained maximum area and flaring activity (Solar-Geophysical Data 1983; McGovern et al. 1981). On the 23rd at least 5 flares occurred, all of sub-X class in soft x-ray flux observed by the GOES spacecraft: early in the day, two class C flares occurred at 0220 and 0239 UT, a class M flare occurred at 0441 UT, and at 1735 and 1745 UT two class C flares occurred. On this day, the active region (a Bp group) had a strong positive magnetic flux area with a full-fledged sunspot preceding westward of several smaller sunspots associated with the negative complex (see Figures 1 and 2).

Questions motivating this case study are:

- (1) To what degree is the magnetic field non-potential on the overall scale of the active region?

(2) What is the size, location, and context of the strongest non-potential features within the active region?

(3) What is the relation of the non-potential features to the flares?

These questions are studied in the context of potential and linear force-free fields computed from the observed photospheric longitudinal field in the active region.

II. OBSERVATIONS

(a) The Coordinated Data Set

For this study we have available a unique coordinated data set consisting of vector magnetograms, H-alpha photographs and high resolution (1") images of the Sun in Lyman-alpha and in the 1600 Å ultraviolet continuum.

The MSFC vector magnetograph (c.f., Hagyard et al. 1982 for a description of the instrument) obtained several maps of the active region between 15:00 and 20:30 UT on 23 September 1980. We have selected for analysis the vector magnetogram obtained at 15:00 UT, the time of best seeing. The spatial resolution of the magnetogram is set by the 2.5" pixel size of the magnetograph. The longitudinal and transverse photospheric magnetic field components were determined in each pixel in the 5' square field of view centered on the active region. The 1-sigma uncertainty in the magnetic field strength is 50 G for the longitudinal field B_l and 75 G for a single component of the transverse field B_t ; these are the standard deviations of the field in the weak field regions of the magnetogram ($|B| < 200$ G).

H-alpha photographs of the active region were taken at the Ottawa Observatory from 19:40 to 20:02 UT. Both line-center and off-band (H-alpha -1.4 \AA) photographs were obtained. The observed H-alpha line center emission originates in the chromosphere at heights of 1,000-10,000 km above the photosphere whereas the line wing at more than 1 \AA from line center is formed much lower, between the photosphere and the temperature minimum (Vernazza, Avrett and Loeser 1981); so, that on the average, much higher structures are seen at line center than in the far wing. The differences between the off-band and line center images are apparent in Figure 1a and 1c.

The Lyman-alpha and 1600 \AA continuum images (Figure 1d and 1b, respectively) are filtergrams obtained by the Transition Region Camera (TRC), a 10 cm diameter telescope, built by the Laboratoire de Physique Stellaire et Planétaire (LPSP) and flown on a NASA Black Brant rocket as part of a collaborative experiment with the Lockheed Palo Alto Research Laboratory (LPARL). These observations have been described in detail by Haisch et al. (1986) and Foing and Bonnet (1984a,b) and references therein. These filtergrams are part of a set of 20 such images, each covering almost the entire solar disk, taken during the ~5 minute rocket flight at ~20:30 UT on 23 September 1980. The Ly-alpha chromospheric images are diffused due to resonant scattering by optically thick coronal hydrogen (Haisch et al. 1986).

The off-band H-alpha (Figure 1a) shows a large, leading sunspot of positive polarity at the top (west) which has a rather

simple configuration. The negative polarity region at the bottom (east) shows a number of smaller, associated sunspots and pores which can be identified with features in the magnetogram of the active region (Figure 2). Figure 2 shows the total magnetic field, the longitudinal field, and the transverse field. The 180 degree ambiguity of the transverse data (c.f., Hagyard et al. 1983) has been resolved by assuming that the transverse field is directed away from the mean center of the positive field and toward one or the other major mean negative centers as determined by minimum distance.

A check on the validity of our vector field measurements can be made by using the following general result for non-linear force-free fields (Aly 1984, Molodensky 1974). For any isolated force-free field having net zero flux, such as an active region, there is the following relation between B_ℓ and B_t on the source surface, taken here to be the x-y plane:

$$\iint |B_\ell|^2 dx dy = \iint |B_t|^2 dx dy \quad (1)$$

i.e., the integrated squared longitudinal field is equal to the integrated squared transverse field on the photospheric surface. The measured net flux in the magnetogram was zero to within the noise. Integration over the magnetogram satisfied Eq. (1) to within 10 percent. This gives us confidence that we measured the field vector reasonably well over the bulk of the active region.


The spot structure is also visible in the 1600 Å image (Figure 1b). The formation of the ultraviolet continuum has been discussed in detail by Haisch et al. (1986), Haisch and Basri (1985), and Foing and Bonnet (1984a,b), in the context of this same data set; by Cook et al. (1983) for a similar set of observations made by the NRL High Resolution Telescope and Spectrograph; and by Vernazza et al. (1976, 1981), Samain (1980), and Avrett (1985) in the context of model atmospheres. It is the temperature minimum region of the solar atmosphere that we are observing at this wavelength--several hundred kilometers above the level of the solar atmosphere seen in Figure 1a. There are numerous discrete bright points that appear at 1600 Å only within the active region; these resemble Ellerman bombs (T. Tarbell, private communication) although there are many more of these bright points at 1600 Å than are seen in the wing of H- α . As a working hypothesis we associate an arbitrary selected set of bright points with footpoints of the observed fibrils (c.f., Kitai and Muller (1984) for a recent discussion of active region fine structure). A bright point and a fibril rooted in or next to the bright point might be consequences of a tiny bipole seated at the bright point.

(b) The Fibril Structure and the Magnetic Field

Fibril structure in the active region is clearly visible in H- α (Figure 1c) and can also be seen in Lyman- α (Figure 1d); presumably the fibrils delineate the magnetic field lines in the chromosphere. We assume that, though individual fibrils

change on a time scale of 20 minutes, the magnetic features delineated at any specific time have a much longer persistence. While the separation of the source layers for Lyman-alpha and H-alpha is not large in a planar model atmosphere (500-1000 km; Vernazza et al. 1981), the actual difference in height of particular H-alpha and Lyman-alpha fibrils varies greatly from case to case and can be much more than 1,000 km. Figures 1a and 1b and other photographs (c.f., Bonnet et al. 1980) clearly show Lyman-alpha emitting magnetic structure at heights greater than 10,000 km--far above the height of formation of Lyman-alpha in a vertically stratified atmospheric model. Typically, H-alpha and Lyman-alpha fibrils are intermixed at heights of 1,000-10,000 km, with the Lyman-alpha fibrils extending somewhat higher than the H-alpha fibrils on the average.

H-alpha and Lyman-alpha fibrils traced from the photographs are drawn on the magnetogram in Figure 3a. Also shown are the position of particular bright points from the 1600 Å continuum photograph; these points were selected as candidate footpoints for the fibrils. The fibrils appear to be fairly flat arches with heights much less than their lengths. This is reasonable because most of the fibrils either span the neutral line and are rooted near the neutral line or are rooted near the sunspots on the side facing the neutral line. Hence the fibrils lie on the field lines that should be predominantly transverse. That the average measured inclination of the photospheric vector magnetic field was 29 degrees for $300 < B < 1000$ G also indicates that maximum height reached should be less than half the span, a rather flat configuration.



Many of the Lyman-alpha fibrils in Figure 4a are longer than the nearby H-alpha fibrils and appear to arch above the H-alpha fibrils. For the most part, neighboring H-alpha and Lyman-alpha fibrils run parallel, but in a few places H-alpha fibrils are definitely crossed by Lyman-alpha fibrils. One such place, which we will call region A, is marked by the arrow in Figure 3a; another is in the lower left quadrant of Figure 3a. The crossing indicates twisting or shearing of the magnetic field with height. Because the Lyman-alpha fibrils to the lower left are longer than those of region A, they probably arch further above the underlying H-alpha fibrils, than those at A. So, the rate of shear with height is probably greater at site A.

We now examine this field structure further by overlaying the photospheric transverse magnetic field vector measurements as shown in Figure 3b. In region A there is a ~ 30 degree rotation between the transverse field and the H-alpha fibrils, and then another ~ 30 degree rotation between the H-alpha fibrils and the Lyman-alpha fibrils. Because the measured photospheric transverse field exceeds 200 G, i.e., is well above threshold, throughout area A and has a uniform direction over this area, we are confident that the measured direction is accurate to better than ± 10 degrees. Other vector magnetograms obtained at MSFC as late as 20:30 UT on the same day showed no detectable change in the magnetic field from that presented here. Region A is exceptional in the degree of difference in alignment both between the H-alpha and Lyman-alpha fibrils and between the fibrils and the transverse photospheric field; in most other areas all three

direction indicators are more nearly aligned. Thus, in region A, the field is apparently more non-potential than in most other areas of the active region.

(c) Flare Sites

Of the five flares that occurred in AR 2684 on this day, we have been able to find H α photographs of only two, the subflares at 1735 UT and 1745 UT. These photographic observations are from the SOON Observatory at Holoman Air Force Base, New Mexico. The H α photograph of the active region at 1745 UT is shown in Figure 4 overlaid with the neutral line and contours of our longitudinal magnetogram.

The flare of 1735 UT was seated in region A. At 1745 UT, this flare was fading in H α brightness but was still noticeable as can be seen in Figure 4. That a flare occurred in region A is further evidence that the magnetic field in region A was non-potential.

The flare of 1745 UT is the other bright feature in Figure 4, the one on the negative polarity side of the major neutral line. As we will show, the magnetic field had a local maximum of non-potentiality in this area comparable in magnitude to that in region A.

III. POTENTIAL FIELD MODEL

We now further examine the non-potentiality of the active region by computing the potential magnetic field from the observed longitudinal field and comparing this potential field

with the observed transverse photospheric field and the observed fibrils.

If one assumes that the field at the photospheric surface and above is potential, then the distribution of the photospheric longitudinal field is sufficient information to determine the vector field everywhere above the photosphere and on the photospheric surface as well. We can therefore directly compare the computed potential transverse field with the observed transverse field; this is done in Figure 5a, where the computed transverse vectors are shown as arrows and the observed transverse vectors are the line segments without arrowheads.

Figure 5a shows that on scales resolved by our magnetograph ($\lambda 4''$), the magnetic field of this active region was only mildly non-potential. That is, although there are significant differences from the potential field, the overall pattern of the observed transverse field in Figure 5a is similar to that of the potential field. The alignment of the observed field with the potential field is closest in and around the large leading sunspot, including region A. The differences in direction between observed and potential transverse vectors are greater along the neutral line and in the following (negative polarity) domain of the active region, but rarely exceed 45 degrees. We also see, that along the neutral line and in the negative polarity domain, the angular deviations of the observed vectors from the potential vectors are predominantly clockwise. This corresponds to net electric current flowing upward through the photosphere in the negative polarity domain and indicates that

the magnetic field was somewhat non-potential on the overall scale of the active region.

We can also use the potential field to examine whether projection effects produced the misalignment between the chromospheric fibrils and the photospheric transverse field seen in region A in Figure 3b. We do this by computing the potential field lines from the assumed footpoints of the observed fibrils, i.e., from the 1600 Å bright points shown in Figure 3. We use the methods of Welck and Nakagawa (1983) and Alissandrakis (1981) for force-free magnetic field computation, and we set $\alpha = 0$ for the potential (current-free) case. These are shown projected onto the photosphere in Figure 5b, and are seen to co-align quite well with the photospheric potential transverse field. Hence the disagreement of the direction of H-alpha and Lyman-alpha fibrils with direction of the photospheric transverse field in region A appears to be non-potential in origin rather than being the result of projection.

Another way to display the non-potentiality of the active region is with the residual field, the observed transverse vector field minus the potential transverse vector field (Hagyard, Low and Tandberg-Hanssen 1981). The greater the residual field, the more non-potential the observed field. The residual field in the interior of the active region is shown in Figure 6. The shortest vectors drawn are for 200 Gauss. Since the uncertainty in the observed transverse field was about 100 Gauss, Figure 6 shows that the magnetic field was measurably non-potential over more than half of the area in the interior of the active region. We

also see that there were three local areas of noticeably enhanced non-potentiality. One of these is region A, the site of the subflare of 1735 UT. Another is the site of the other subflare shown in Figure 4, the one that occurred at 1745 UT. The third and strongest area of non-potentiality covers the bend in the neutral line in the lower part of Figure 6. We do not know if this was the site of any of the other three flares that occurred in the active region on this day.

IV. NON-POTENTIAL FORCE-FREE MODEL

(a) Predicted versus Observed Transverse Field

The observation of the transverse field allows calculation of the electric vertical current density. Calculation of the vertical electric current density from the transverse vector field measurements (i.e., $\frac{\partial B_x}{\partial y} - \frac{\partial B_y}{\partial x} = \mu_0 J_z$) has been carried out by a number of authors (Moreton and Severny 1968; deLoach et al. 1983; Krall et al. 1982; Hagyard, West, and Smith 1984). The electric current calculated for this region has been given by Haisch et al. (1986). However the limited spatial resolution and measurement noise for the transverse field limit the range of current density that can be detected. The size of the individual electric current elements could be well below the resolution of the magnetograph (Rabin and Moore 1985). In any case, fine-scale magnetic structures below the resolution of the magnetograph (~4") can affect the global field of an active region. In addition, horizontal currents cannot be directly calculated at all from photospheric vector magnetograms alone. But, the effect

of the total current system, the sum of both the vertical and horizontal components, can be seen in the pattern of the observed photospheric transverse field (c.f. Hagyard, Low, and Tandberg-Hanssen 1981). Here we study this total effect of the current system by examining the observed photospheric transverse field pattern and the observed fibril pattern for differences and agreement with constant α non-potential force-free fields.

We now apply the force-free model to calculate constant- α fields; in Figure 7 we show an intercomparison of the predicted transverse photospheric magnetic field derived from the observed longitudinal field and the assumption of a constant α for the potential case ($\alpha = 0$) and for two non-potential cases, $\alpha = -1.0$ and -2.0 in units of $2\pi/L = 0.27 \times 10^{-7} \text{ m}^{-1}$, where L is the size of the magnetogram on the Sun in kilometers. (The procedure of Alissandrakis (1981) was employed for $|\alpha| > 1$ with the field decreasing exponentially with z .) Negative values of α are required to produce twist in the same direction as that seen in the observed field (Figure 2d) and noted in Figure 5a. Comparing the predicted transverse field for $\alpha = -2.0$ with the observed transverse field (see Figure 2d), we find that the overall twist of the observed field is clearly less than that of the $\alpha = -2.0$ field; this implies an upper limit to the average large scale current density of $8.6 \times 10^{-4} \text{ amps m}^{-2}$ for the total region, assuming an average field of 200 Gauss. This current density is an upper limit for the overall net current in this active region and is an order of magnitude less than the localized peak values found directly from the curl of B in this active region by Haisch et al. (1986).

The value of $\alpha = -1.0$ gives a transverse field twist comparable to that of the observed transverse field (Figure 2d). This corresponds to an average net current density of order 4×10^{-4} amp m^{-2} and a total net current of order 3×10^{12} amp flowing from the negative polarity domain to the positive polarity domain of the active region.

(b) Effect of Alpha on Field Lines

Next we take a range of α of ± 1.0 ($= \pm 0.27 \times 10^{-7} m^{-1}$) and look more closely at the effect of α on the angular rotation of the predicted transverse field at each point. In Figure 8a we show the transverse azimuth variation for $\alpha = -1.0$ and $+1.0$. This shows that the azimuth direction for these values of α can vary by as much as 20 degrees from the potential field direction. This is comparable to the range of angles seen for the observed field in Figure 5a. In Figure 8b we show the effect of this same range of α on the projected field lines, which again have been generated at the selected footpoints corresponding to the 1600 Å bright points.

(c) Sign-of- α Maps

We can use the above azimuth dependency on α to assign the sign of alpha corresponding to the direction of the observed transverse field point by point in the active region. In Figure 9a a "sign-of- α " map has been generated; this was done by comparing the observed azimuth of the transverse field (i.e., the direction only) with the potential field. This method of determining the sign of α differs from the more direct method whereby the presence of photospheric currents is inferred

directly from the measured curl of \mathbf{B} , as in Haisch et al. (1986) and deLoach et al. (1984). Here the sense (sign) of the twist is determined for each point individually. We have limited ourselves to regions where the transverse magnetic measurements are well determined (>250 G), though the central umbrae areas are ignored.

Yet another inference of the sign of α can be obtained by comparing the fibril structure with field lines calculated from constant alpha force-free models. For this, we have used another set of projected field lines (similar to those shown in Figure 8b, except for somewhat smaller values of alpha: $\alpha = -0.5, 0.00, +0.5$) and have compared these with the H-alpha and Lyman-alpha fibril structure. Our results are shown in Figure 9b wherein regions showing agreement between the predicted field and fibril orientations are outlined as a function of the sign of α .

The photospheric sign-of- α map in Figure 9a confirms our inferences drawn from inspection of the superposition of the observed photospheric transverse field and the potential transverse field in Figure 5a. In both of these Figures, we see that there was no discernible overall twist in the field in and around the large leading positive polarity sunspot. Figure 9a also shows the extent to which the sense of twist corresponding to negative alpha predominated along the neutral line and in the negative polarity domain of the active region.

The chromospheric sign-of- α map in Figure 9b shows predominance of negative α on both sides of the neutral line in the interior of the active region. Thus, the chromospheric

fibrils show an overall twist that agrees in sign with the predominant twist seen in the photospheric field. This result is expected for net large scale current flowing along the field lines but in the opposite direction, i.e., from the negative polarity domain to the positive polarity domain of the active region.

(d) Residual Field for the Constant-Alpha Model

In Figure 10a we show the transverse field for the constant-alpha model having $\alpha = -0.5$. In Figure 10b we show the residual field for this model, obtained by subtracting the potential field. There is a clear pattern of overall twist or circulation in the residual field in each of the two opposite polarity domains of the active region. This pattern is characteristic for constant- α models; the residual field for $\alpha = -1.0$ is twice as strong as in Figure 10b but has the same pattern.

The actual residual field of the active region, shown in Figure 6, has much more small-scale structure than for a constant- α model. This demonstrates that, although there is a predominant direction of twist in the active region, the value of α is far from constant over the active region.

V. NON-POTENTIAL ENERGY IN THE OBSERVED FIELD

For any force-free field of limited spatial extent, as for an active region, the total energy ϵ of the field above the photosphere is given by the following integral of the photospheric vector field (Low 1982b):

$$\epsilon = \frac{1}{4\pi} \iint B_z (xB_x + yB_y) \, dx dy, \quad (2)$$

where the z axis is vertical. Evaluation of this integral over our magnetogram gives

$$\epsilon_{\text{observed}} = 1.96 \times 10^{33} \text{ erg.}$$

For the potential field computed from the observed longitudinal component of the photospheric field, the integral gives

$$\epsilon_{\text{potential}} = 1.76 \times 10^{33} \text{ erg,}$$

which indicates that the non-potential magnetic energy in the active region was of order 10^{32} erg.

Evaluation of the integral with 3σ perturbations of the potential field vector, i.e., perturbations 3 times larger than the observed noise levels in the longitudinal and transverse components, gives

$$\begin{array}{l} \epsilon_{\text{potential}} \\ \text{with } 3\sigma \text{ noise} \end{array} = 1.95 \times 10^{33} \text{ erg.}$$

Thus, the measured non-potential magnetic energy was well above the noise, and was probably an order of magnitude more than all the energy released in the flares that occurred in this active region on this day. This result also indicates that the present noise level in our vector field measurements probably prohibits

direct measurement of the energy extracted from the field by a flare except for the very largest flares, in which the total energy released is of order 10^{32} erg. Reduction of the noise level in the vector measurements by an order of magnitude, as could be achieved by a vector magnetograph of higher resolution, e.g. in space, may allow direct measurement of the magnetic energy change in many flares. But the total net current of an active region can provide a measurable lower limit of the energy, as obtained above.

VI. SUMMARY AND CONCLUSIONS

We have intercompared a unique coordinated data set consisting of vector magnetograms, H-alpha photographs, and high resolution ultraviolet images of an active region. Using these data and mathematical models to calculate potential and force-free magnetic field lines we have examined the non-potential nature of the active region structure.

(1) Our measurements of the photospheric magnetic field in this active region satisfied to within 10% the theoretical requirement for any isolated force-free field that the area integrals of the squares of the transverse and longitudinal field components be equal. This is an indication that the field in this active region was in fact nearly force free and that the bulk of the large-scale photospheric vector field was correctly measured.

(2) The observed photospheric transverse field and the H-alpha and Ly-alpha chromospheric fibrils were all roughly aligned

with each other and with the potential field calculated from the observed longitudinal field. However, there were clear examples of definite non-potential differences between the photospheric transverse field and the chromospheric fibrils and between the H-alpha and Ly-alpha fibrils. In one area there was a ~30 degree rotation between the photospheric transverse magnetic field and the H-alpha fibrils; and another ~30 degree rotation between the H-alpha and Lyman-alpha fibrils. This was a flare site.

(3) Comparison of the observed photospheric transverse field with the computed potential transverse field showed that, along the neutral line and in the negative polarity half of the overall bipole, the observed field on average had a clockwise rotation with respect to the potential transverse field. This overall twist was confirmed both by the sign-of- α map for the observed photospheric field and by the sign-of- α map constructed from the observed chromospheric fibrils. The direction of the net twist corresponded to net current arching over the neutral line by flowing anti-parallel to the magnetic field lines. The average density of this net current was of order 4×10^{-4} amp m^{-2} and the total net current was of order 3×10^{12} amp.

(4) The map of the residual field, i.e., the difference between the observed photospheric transverse field and the potential transverse field, and the sign-of- α maps showed that the non-potentiality of the observed field had much more structure than for a constant- α field. Alpha changed sign over the active region, and the observed residual field pattern had little resemblance to a constant- α residual field even in the

regions where α kept one sign.

(5) The observed residual field showed three areas of enhanced non-potentiality in the interior of the active region. One of these was the site of the clear rotation of the field direction with height. Within a few hours of the field observations, a flare occurred in this area and another flare occurred in one of the other areas of enhanced non-potentiality.

(6) The total non-potential energy present in the active region was measured to be of order 10^{32} erg, ample for the five small flares that occurred in this active region over that day, but only 3σ above the measurement noise. This shows that to measure the magnetic energy changes wrought by any but the largest flares require much improvement in the accuracy of the vector field measurements. A major hindrance to measurement accuracy is the known subarcsecond structure of the photospheric field and the seeing-limited resolution of about $1''$, at best, that can routinely be achieved in magnetograms from the ground at the best observing sites. This indicates the need for a vector magnetograph in space.

Acknowledgments

This work was supported by the NASA Office of Solar and Heliospheric Physics and by the Air Force Geophysical Laboratory through its Solar Research Branch of the Space Physics Division. The authors thank Vic Gaizauskas, Herzberg Institute of Astrophysics, National Research Council, Ottawa for the H-alpha photographs of Figure 1, and Vi Miller, Space Environment Laboratory, NOAO, for the SOON photograph of Figure 4.

References

- Ai, G. and Kong, F. 1983, Chinese Astr. Ap., 7, 6.
- Alissandrakis, C. E. 1981, Astron. Astrophys., 100, 197.
- Avrett, E.H. 1985, in "Chromospheric Diagnostics and Modeling,"
B. W. Lites (ed.).
- Barnes, C. W. and Sturrock, P. A. 1972, Ap. J., 174, 659.
- Basri, G. S., Linsky, J. L., Bartoe, J.-D. F., Brueckner, G., and
Van Hoosier, M. E. 1979, Ap. J., 230, 924.
- Bonnet, R. M., Bruner, E. C., Acton, L. W., Brown W. A., and
Decaudin, M. 1980, Ap. J. (Letters), 237, L47.
- Bonnet, R. M. and Tsiropoula, G. 1982, Solar Phys., 75, 139.
- Chiu, Y. T. and Hilton, H. H. 1977, Ap. J., 212, 873.
- Cram, L. E., Nye, A. H. and Thomas, J. H. 1981, in "The Physics
of Sunspots", Cram, L.E. and J. H. Thomas (eds.) (Sacramento
Peak Observatory).
- Cook, J. W., Brueckner, G. E., and Bartoe, J.-D. F. 1983, Ap. J.
(Letters), 270, L89.
- deLoach, A. C., Hagyard, M. J., Rabin, D., Moore, R. L., Smith,
J. B., West, E. A., and Tandberg-Hanssen, E. 1984, Solar
Phys., 91, 235.
- Foing, B., and Bonnet, R. M. 1984a, Ap. J., 279, 848.
- Giovanelli, R. G. and Jones, H. P. 1982, Solar Phys., 79, 267.
- Hagyard, M., Low, B. C., and Tandberg-Hanssen, E. 1981, Solar
Phys., 73, 257.
- Hagyard, M., Cumings, N. P., West, E. A., and Smith, J. E. 1982,
Solar Phys., 80, 33.

- Hagyard, M., Smith, J. B., Teuber, D. L., and West, E. A.
1984, *Solar Phys.*, 91, 115.
- Hagyard, M., West, E. A. and Smith, J. B., Jr. 1983 ,in
"Proceedings of the Solar Physics and Interplanetary
Travelling Phenomena"(Kunming, People's Republic of China).
- Haisch, B. M. and Basri, G. 1985, *Ap. J. (Suppl.)*, 58, 179.
- Haisch, B. M., Bruner, M. E., Hagyard, M. J., and Bonnet, R. M.
1986, *Ap. J.*, 300, 428.
- Hannakam, L., Gary, G. A., and Teuber, D. L. 1984, *Solar Phys.*,
94, 219.
- Harvey, J. 1977, in "Highlights of Astronomy", vol. 4, part II,
E. A. Muller (ed.), p.223.
- Holman, G. D. and Kundu, M. R. 1985, *Ap. J.*, 292, 291.
- Kang, Z. and Lin, Y. 1983, in "Proceedings of the Kunming
Workshop on Solar Physics and Interplanetary Travelling
Phenomena," Kunming, People's Republic of China.
- Krall, K. R, Smith, J. B., Jr., Hagyard, M. J., West, E. A., and
Cummings 1982, *Solar Phys.*, 79, 59.
- Kitai, R. and Muller, R. 1984, *Solar Phys.*, 90, 303.
- Kotov, V. A. 1971, in "Solar Magnetic Fields", R. Howard (ed.),
(IAU Symp.43), (Dordrecht: Reidel).
- Levine, R. H. 1975, *Solar Phys.*, 44, 365.
- Levine, R. H. 1976, *Solar Phys.*, 46, 159.
- Low, B. C. 1982a, *Rev. Geophys. Space Sci.*, 30, 421.
- Low, B. C. 1982b, *Solar Phys.*, 77, 43.
- Ma, E. and Ai, G. 1980, *Chinese Astr. Ap.*, 4, 366.

- McGovern, J. G., Speich, D. M., Nelson, J. J., and Pryor, L. H.
1981, Solar Maximum Mission Active Region Histories and
Synoptic Observations, SMM Report.
- Meyer, R. X., et al. 1976, in "Scientific Experiments of Skylab"
(AIAA/AGU Conference 1974, Progress in Astron. and Aeron.,
vol. 48), AIAA, p. 161.
- Molodensky, M. M. 1974, Solar Phys., 39, 393.
- Moreton, G. E. and Severny, A. B. 1968, Solar. Phys., 3, 282.
- Nakagawa, Y. et al. 1971, Solar Phys., 19, 72.
- Nakagawa, Y. and Raadu, M. A. 1972, Solar Phys., 127, 135.
- Nakagawa, Y. Raadu, M. A., and Harvey, J. M. 1973, Solar Phys.,
30, 421.
- Orrall, F. Q. (ed.) 1981, "Solar Active Regions" (Boulder:
Colorado Associated University Press).
- Rabin, D. and Moore, R. 1985, Ap. J., 285, 359.
- Pridmore-Brown, D. C. 1981, Rpt. ATR-81 (7813)-1, Aerospace
Corporation, El Segundo, CA.
- Priest, E. R. 1982, "Solar Magnetohydrodynamics" (Dordrecht:
Reidel).
- Richardson, R. S. 1941, Ap. J., 93, 24.
- Sakurai, T. 1979, Publ. Astron. Soc. Japan, 31, 309.
- Sakurai, T. 1981, Solar Phys., 69, 343.
- Sakurai, T. 1982, Solar Phys., 76, 301.
- Samain, D. 1980, Ap. J. (Suppl.), 44, 273.
- Schmidt, H. U. 1964, in "Physics of Solar Flares", NASA SP-50,
p.107.
- Seehafer, N. 1985, ~~Solar~~ Phys. 96, 307.

- Simon, G. and Wilson, P. R. 1983, Ap. J., 273, 805.
- Simon, G. and Wilson, P. R. 1985, Ap. J., 295, 241.
- Smith, S. F. and Howard, R. 1968, in "IAU Symp. 35", p.34,
(Dordrecht: Reidel).
- Solar-Geophysical Data 1983, Comprehensive Reports, Number 463,
Part II, NOAA, National Geophysical Data Center, Boulder,
Colorado.
- Stenflo, J. O. 1976, in "Basic Mechanisms in Solar Activity",
Bumba and Kleczek (eds.), p. 69.
- Stenflo, J. O. 1983, "Solar and Stellar Magnetic Fields: Origins
and Coronal Effects" (Dordrecht; Reidel).
- Vernazza, J. E., Avrett, E. H. and Loeser, R. 1976, Ap. J.
(Suppl.), 30, 1.
- Vernazza, J. E., Avrett, E. H. and Loeser, R. 1982, Ap. J.
(Suppl.), 46, 635.
- Wellck, R. E. and Nakagawa, Y. 1983, NCAR-TN/STR-87.
- Woltier, L. 1958, Proc. Nat. Acad. Sci., 44, 489.
- Wu, S. T., 1984, private communication.
- Yang, H-S and Zhang, H-M. 1981, Chinese Astr. Ap., 5, 77.

Figure Captions

Figure 1. The active region 2684 on 23 September 1980 is shown in the left half of four photographs: (a) Off-band H-alpha ($H\text{-}\alpha - 1.4 \text{ \AA}$) taken at 20:02 UT by Herzberg Institute of Astrophysics (HIA). (b) UV-continuum (1600 \AA) taken between 20:25-20:30 UT by the LPSP TRC. (c) Line-center H-alpha taken at 19:40 UT by HIA. (d) Lyman-alpha taken in the same time frame as (b). The region shown is $200'' \times 260''$. The box in (a) is the area studied in this paper. Selected bright points from (b) and fibrils from (c) and (d) are shown in Figure 3. West is up and south is to the right.

Figure 2. The MSFC vector magnetograph data (15:05-15:10 UT) is displayed as: (a) the total magnetic field intensity contours at intervals of 250 G, (b) the longitudinal magnetic field contours at 200 G intervals with the negative contours dashed and the first solid contour at 0 G being the neutral line (c.f. with (d)), (c) contours of the transverse field strength at 100 G intervals starting 200 G, and (d) the transverse vector field above 200 G with the B_z neutral line. The field of view here ($125'' \times 200''$) is the box in Figure 1a; the magnetic data are from a subsection of the full ($640'' \times 640''$) magnetogram. The tick marks along the edges of the panels here and in subsequent Figures are $2.5''$ apart and are centered on rows or columns of pixels in the magnetogram. The large sunspot in Figure 1a is the strongest positive region.

Figure 3. (a) The fibril structure of the H-alpha (----) and Ly-alpha (—) observations of Figure 1 and selected bright

points (o) seen in the uv-continuum (1b) are shown superposed on the longitudinal magnetic field configuration. The 500 Gauss contours and the neutral line (i.e., the zero B_z contour) are shown. In (b) the transverse magnetic field vectors are shown ($B_t > 200$). In the region pointed to by the arrow in (a) (region A in Figure 5), the progressive change in direction from the photospheric transverse field to the H-alpha fibrils to the Lyman-alpha fibrils indicates a twisting of the magnetic field with height. In most other regions, the directions of these three indicators are more nearly aligned. This indicates that the field in region A is more non-potential than in most other areas of the active region.

Figure 4. H_α photograph of the active region at 1745 UT, with the neutral line and contours from our longitudinal magnetogram superposed. Two small flares are in progress. One, near the leading sunspot, is in the area of non-potential field pointed out in Figure 3. The other flare is near a trailing sunspot; our measurements of the photospheric vector magnetic field show that the field in this area was also markedly non-potential. The photograph is from the SOON Observatory at Holloman Air Force Base. The field of view in this Figure is 90"x165".

Figure 5. (a) Comparison of the computed potential transverse field with the observed transverse field. The potential vectors are those with arrowheads. The observed field is seen to be only mildly non-potential. The larger departures in direction from the potential field are along the neutral line

and in the negative polarity half of the active region and are predominantly clockwise. The length of the vector is proportional to the strength of the transverse field; the shortest vectors shown are for 200 Gauss. No transverse field is shown in the central areas of the sunspots where the longitudinal field exceeds 1500 Gauss, because the darkness of the umbra in combination with the scattered light in the magnetograph make the transverse field measurements suspect there. (b) The potential field lines as calculated from the longitudinal field are seen projected unto the photosphere. The field line projections are seen to be aligned fairly well with the transverse potential field vectors of the photosphere. In particular, there is good alignment in region A. The footpoints for the field line are at selected UV-continuum bright points.

Figure 6. The residual field (\equiv observed field minus potential field) in the interior of the active region. The lower cutoff value is 200 Gauss. The observed field is most non-potential in the areas where the residual field is greatest. Two of the three strongest local maxima in the residual field are the sites of the two subflares shown in Figure 4.

Figure 7. The transverse vector field for constant alpha force-free field models (c.f., Alissandrakis 1981) for alpha values of (a) $\alpha = 0.0$ (potential), (b) $\alpha = -1.0$, and (c) $\alpha = -2.0$. The alpha value units are $0.27 \times 10^{-7} \text{m}^{-1}$. Negative values of α produce the direction of overall twist seen in the observed field; $\alpha = -1.0$ produces roughly the observed magnitude of twist (see Figures 2d and 5a).

Figure 8. (a) The range of directions of the computed transverse vector field for $\alpha = +1$ to -1 (b) The variation of the field line trajectories for $\alpha = +1, 0.0$, and -1 for a selected subset of footpoints (cf. Figure 5b).

Figure 9. (a) The sign-of-alpha map generated by comparing the observed photospheric transverse field azimuth direction with the potential ($\alpha = 0$) field direction. The observed transverse field cutoff is 250 G. The $\alpha = 0$ bandwidth used was 0.04. (b) Sign-of-alpha map generated by comparing the fibril structure of H-alpha and Ly-alpha with constant- α field line projections. The sign-of-alpha values was decided according to which of three computed field lines (for $\alpha = -0.5, 0.0$, and 0.5) aligned best with the observed fibrils at the same site. Alignment worse than 45 degrees for all three lines is called "no match" and is indicated by cross hatching. These maps confirm our inference from Figure 5a that the field in the interior of the active region had a net overall twist corresponding to net current flowing anti-parallel to the magnetic field.

Figure 10. (a) Transverse field for the constant-alpha model with $\alpha = -0.5$. (b) The residual field obtained by subtracting the potential field from constant-alpha non-potential field in (a). The minimum transverse fields shown are 200 Gauss in (a) and 50 Gauss in (b). Comparison of the residual field pattern in (b) with that of the actual residual field in Figure 6 shows that the α of the observed field is far from constant over the active region.

Authors

Dr. G. A. Gary
ES52
Marshall Space Flight Center
Marshall Space Flight Center, AL 35812

Dr. R. L. Moore
ES52
Marshall Space Flight Center
Marshall Space Flight Center, AL 35812

Dr. M. J. Hagyard
ES52
Marshall Space Flight Center
Marshall Space Flight Center, AL 35812

Dr. Bernhard M. Haisch
Lockheed Palo Alto Research Laboratory
Palo Alto, CA 94304



(a)



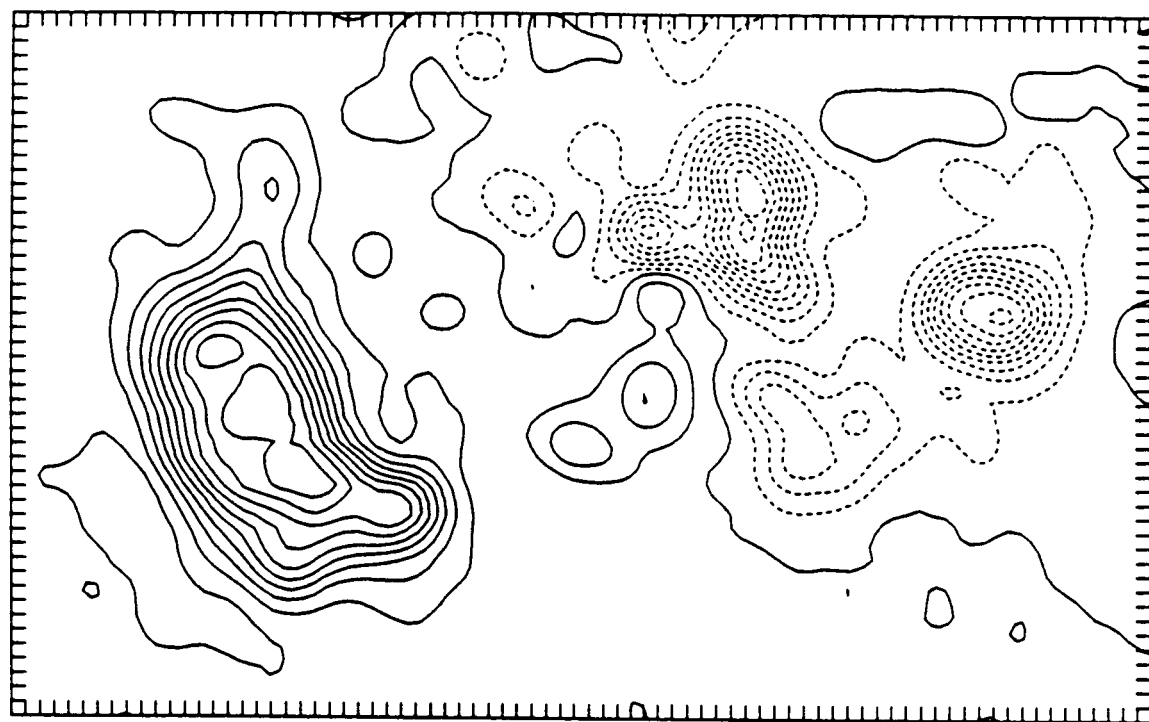
(b)



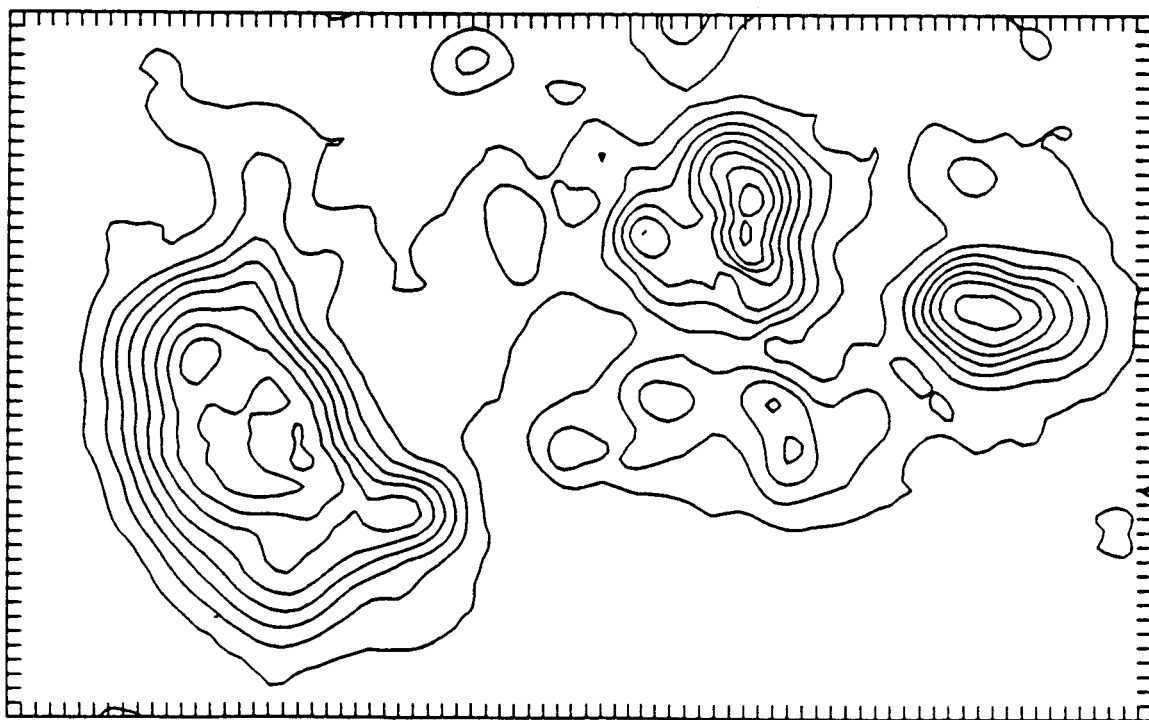
(c)



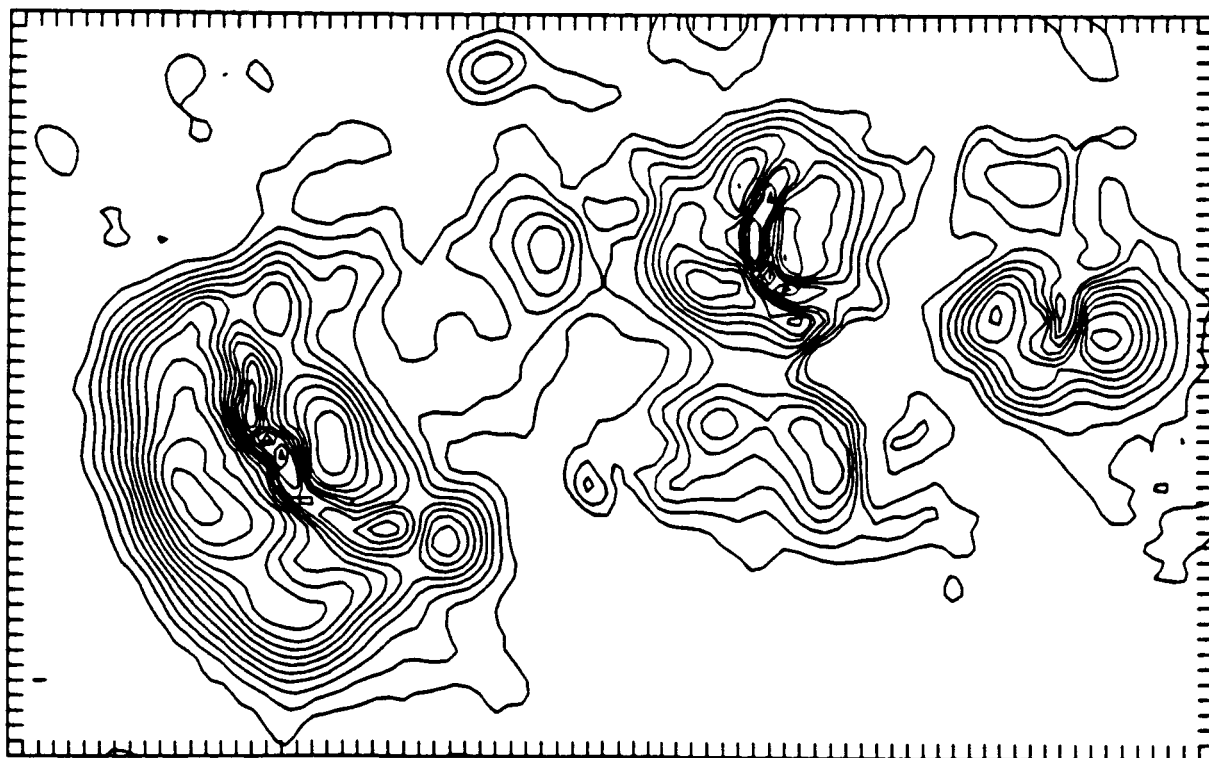
(d)



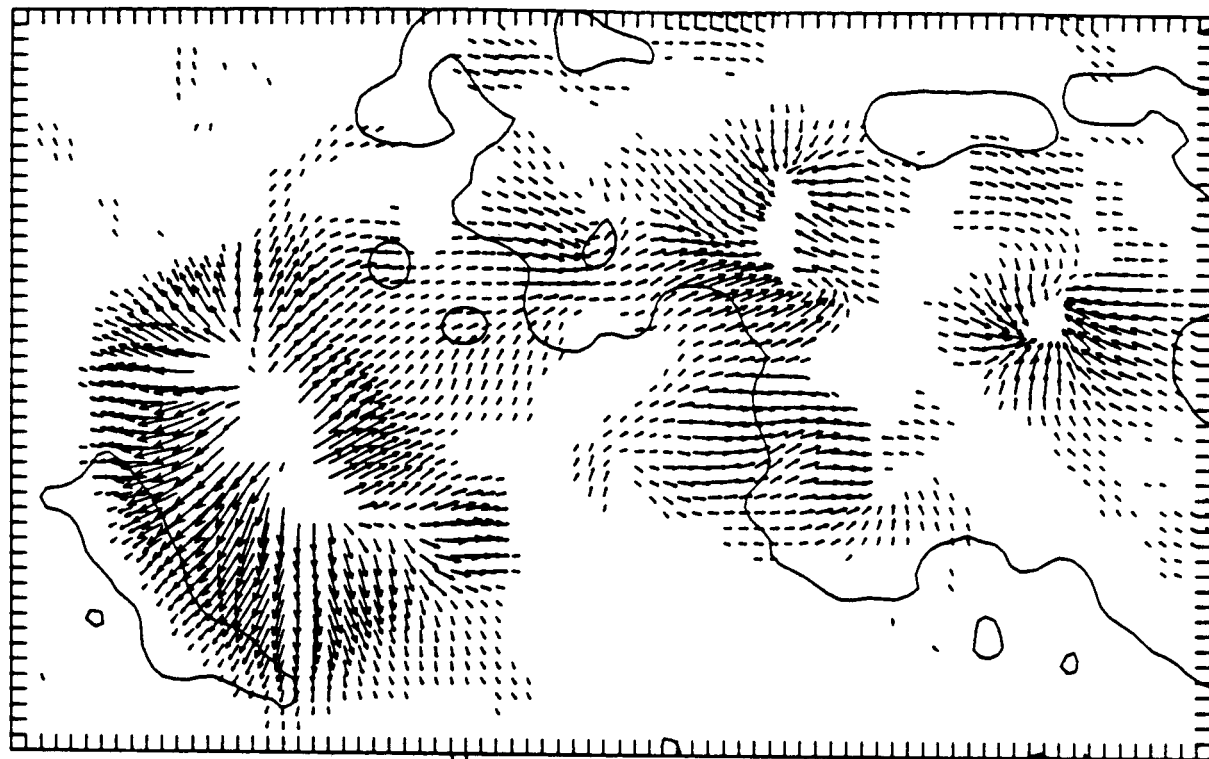
(b)



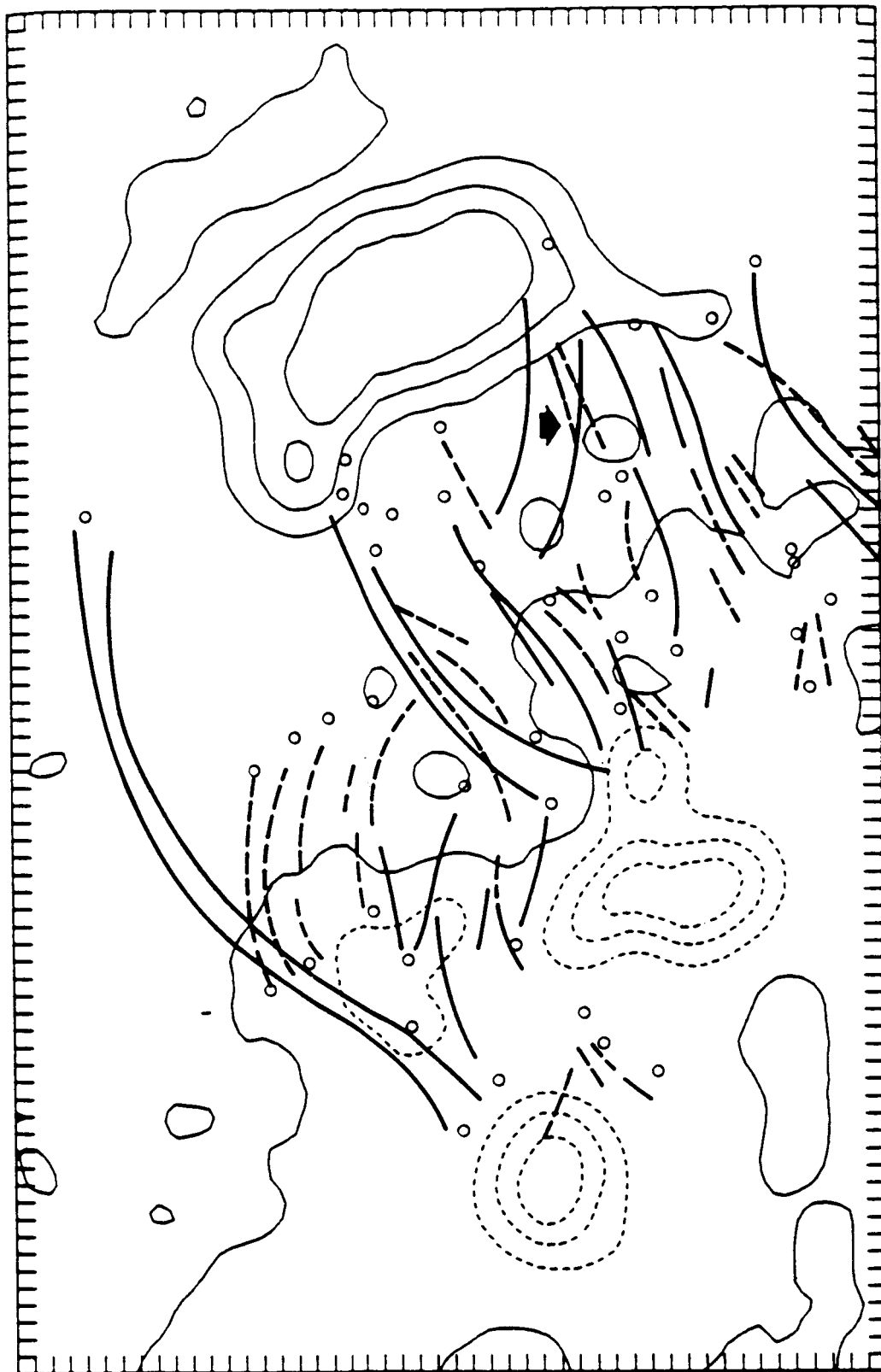
(a)



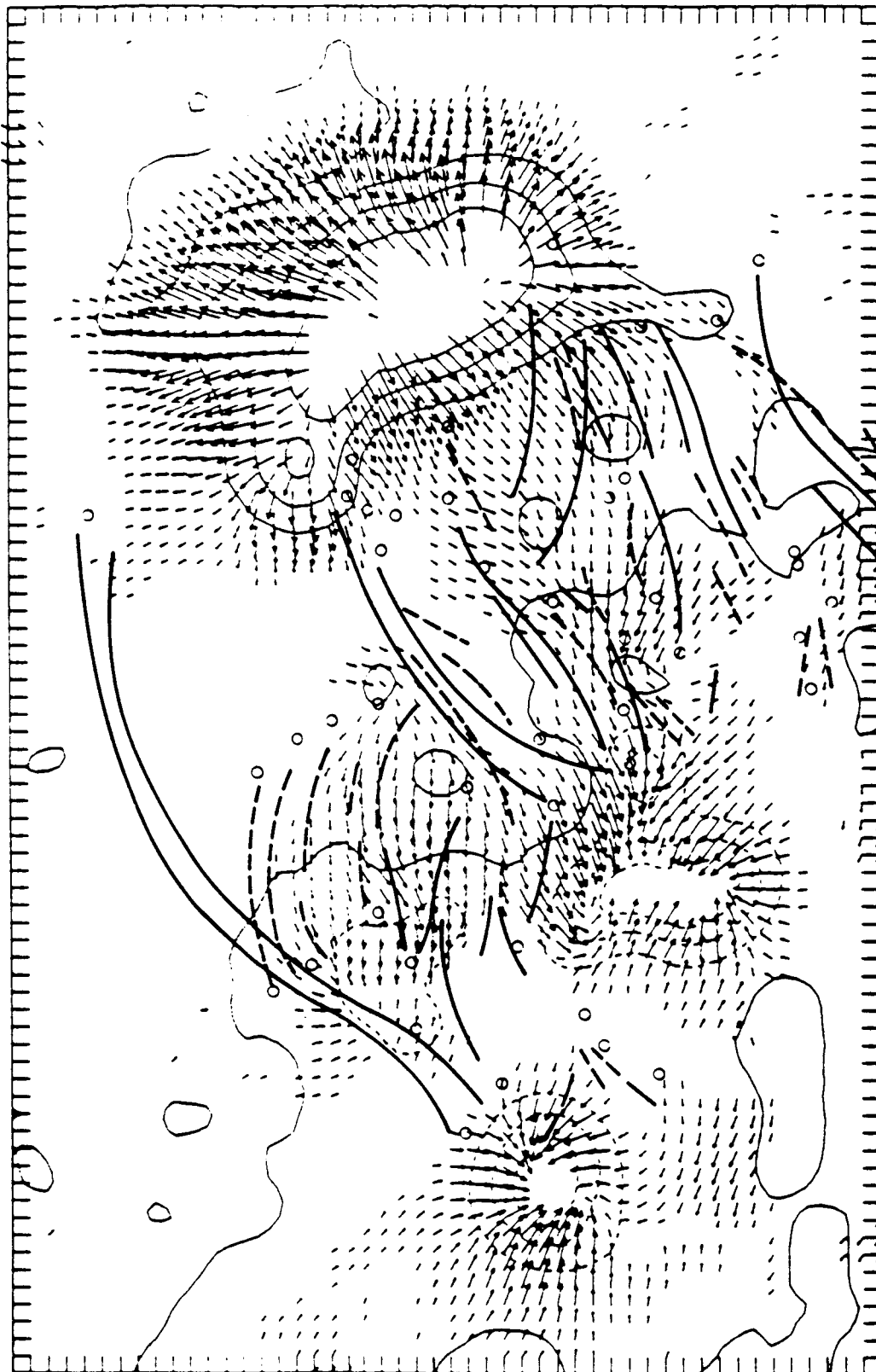
(c)



(d)



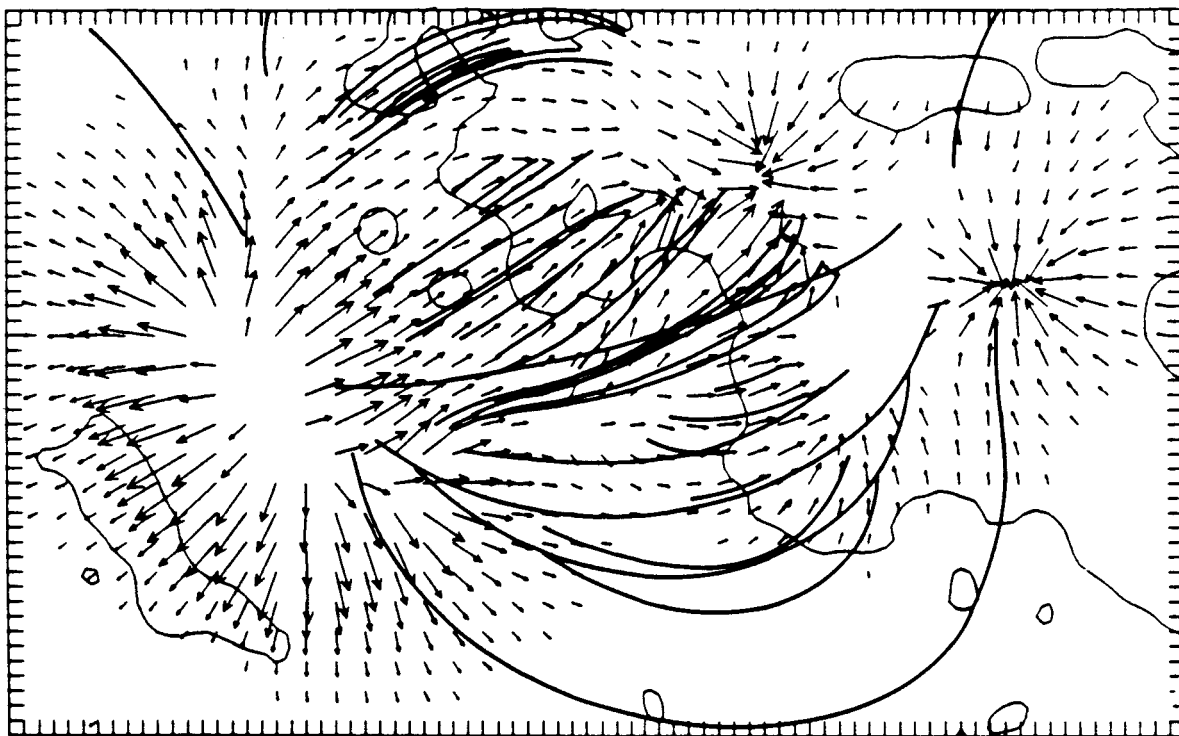
(a)



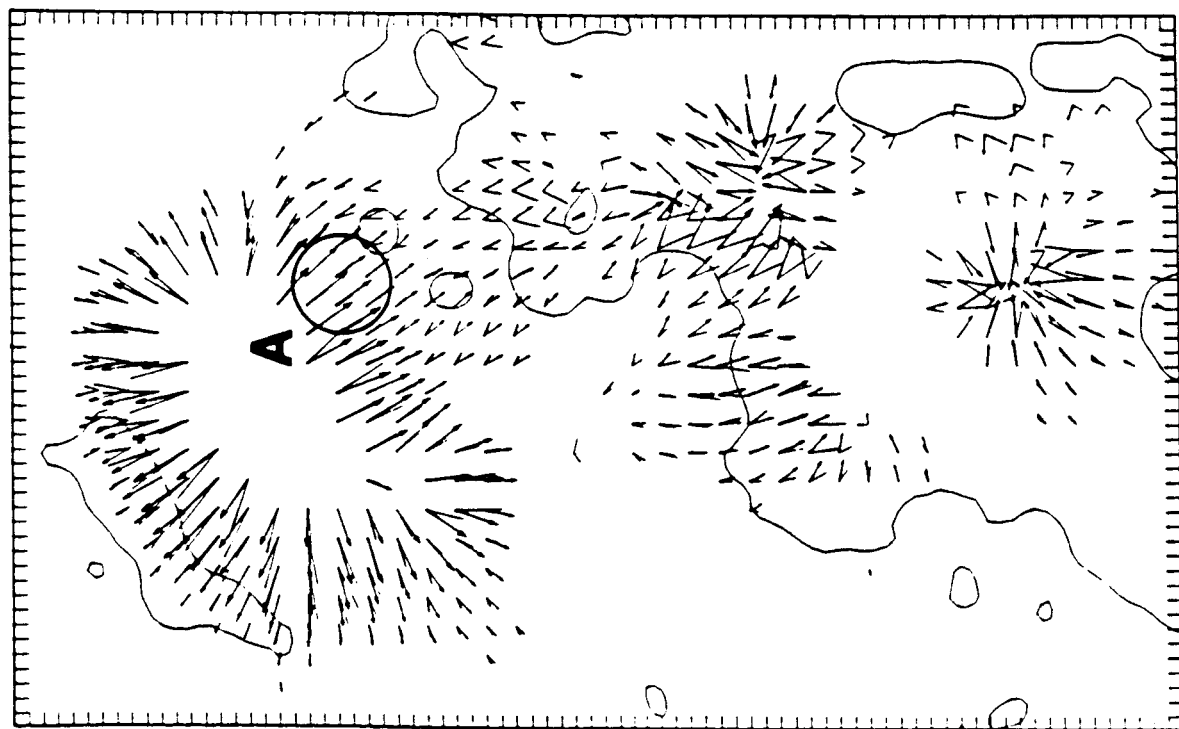
(b)



Fig 4



(b)



(a)

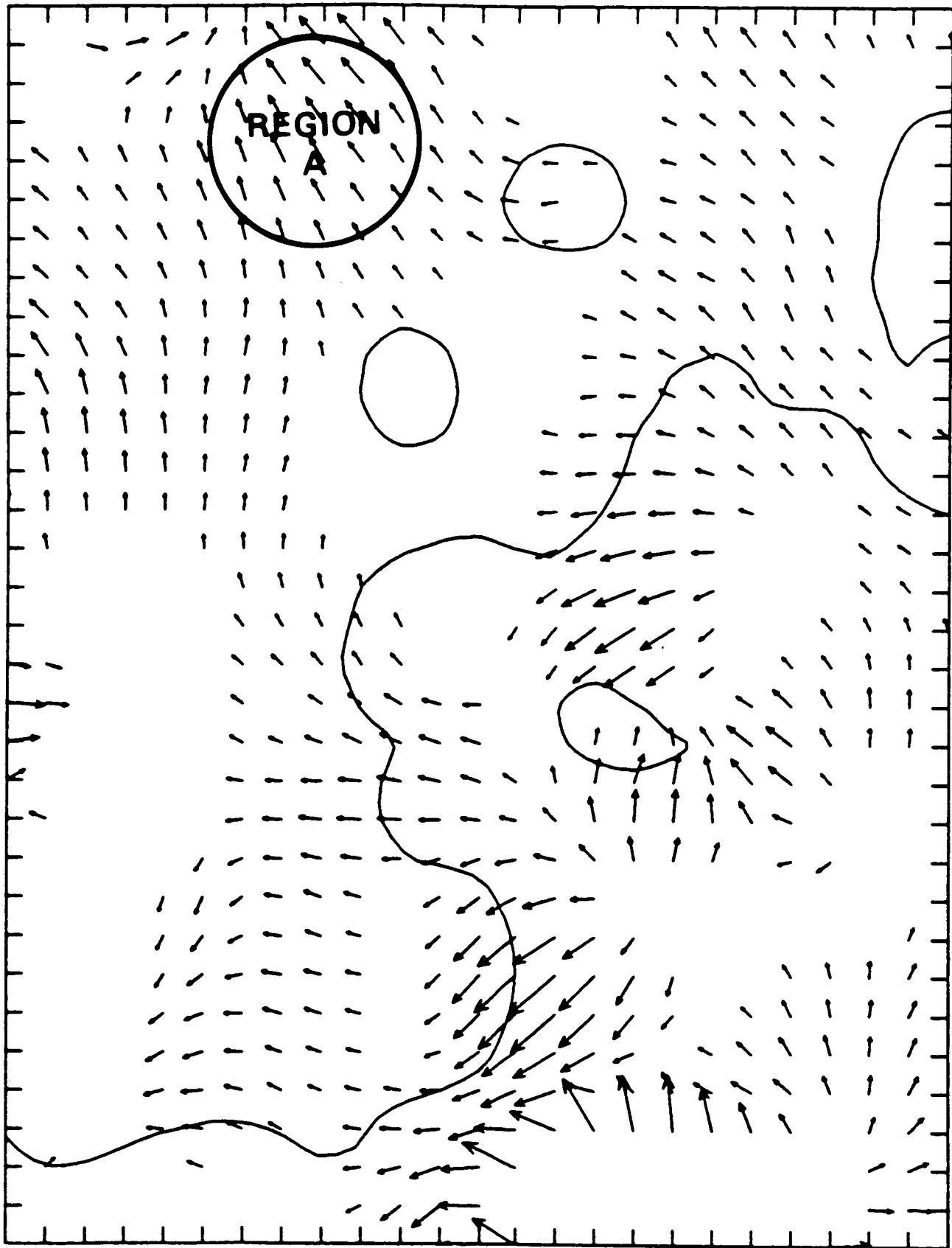
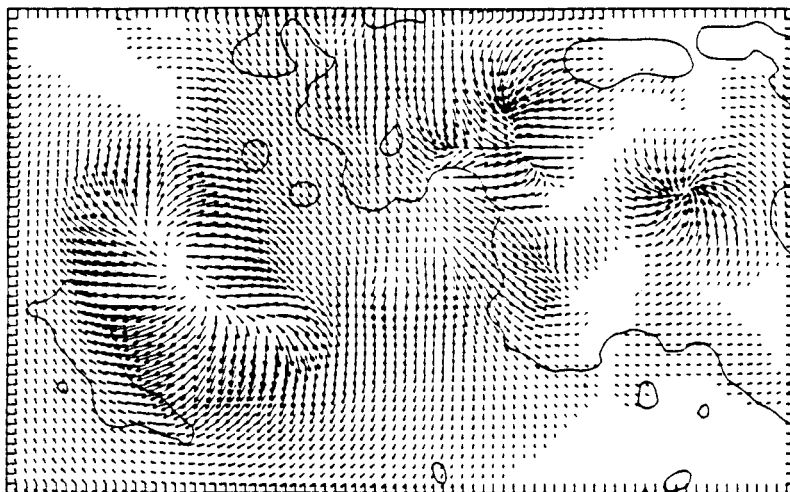
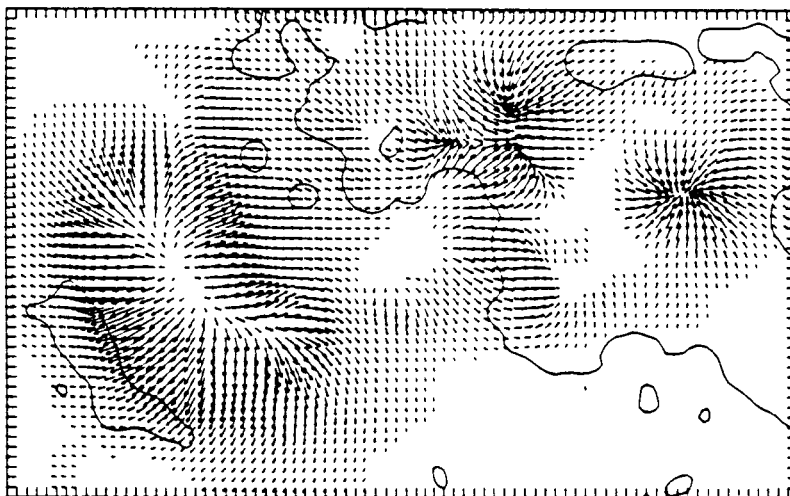


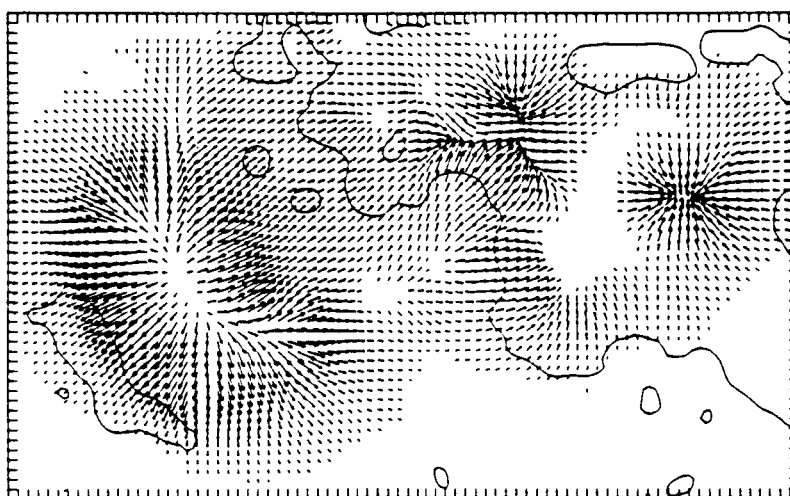
Fig 6



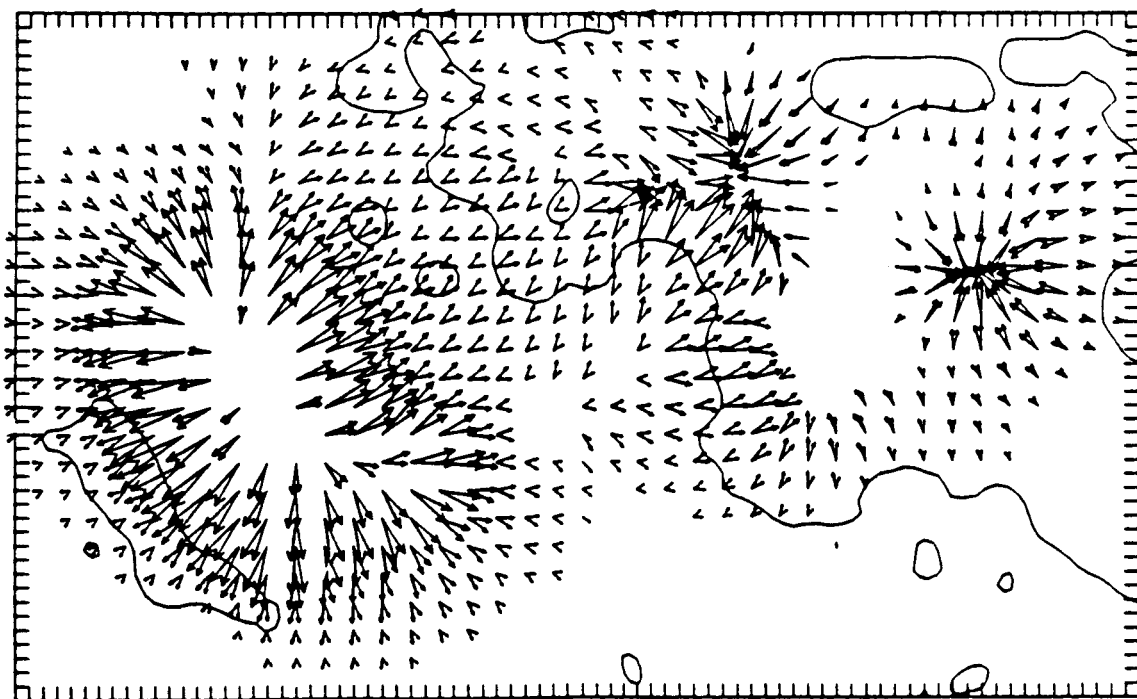
(c)



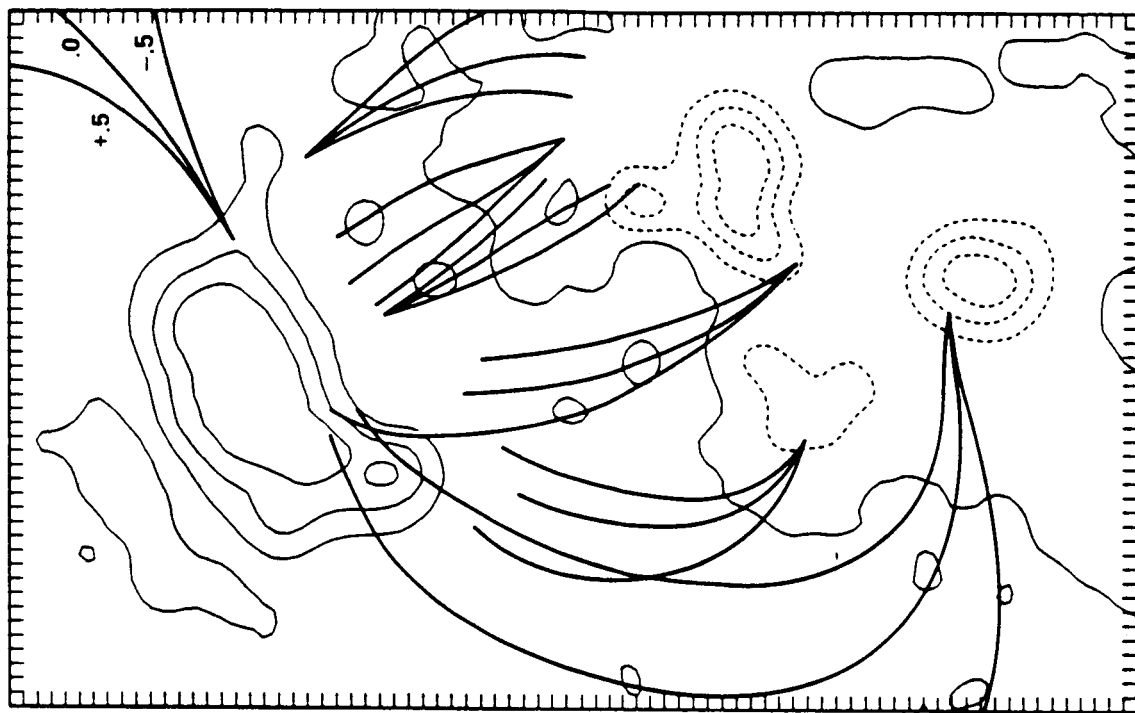
(b)



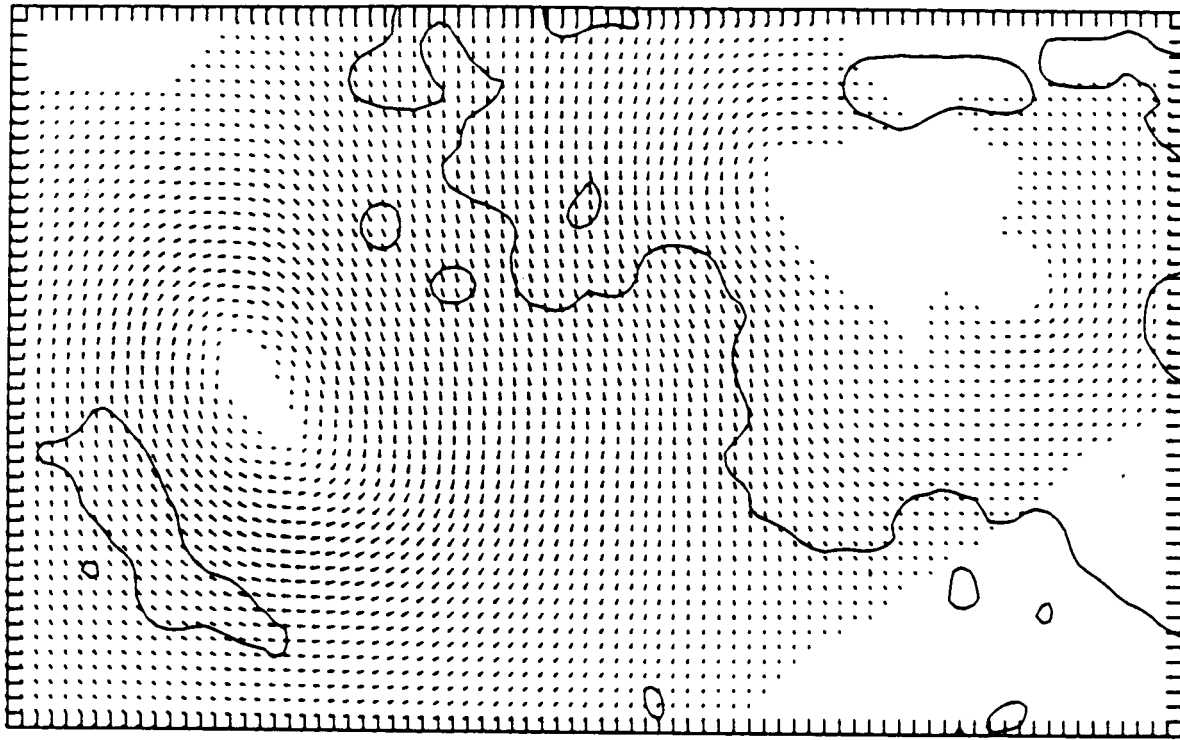
(a)



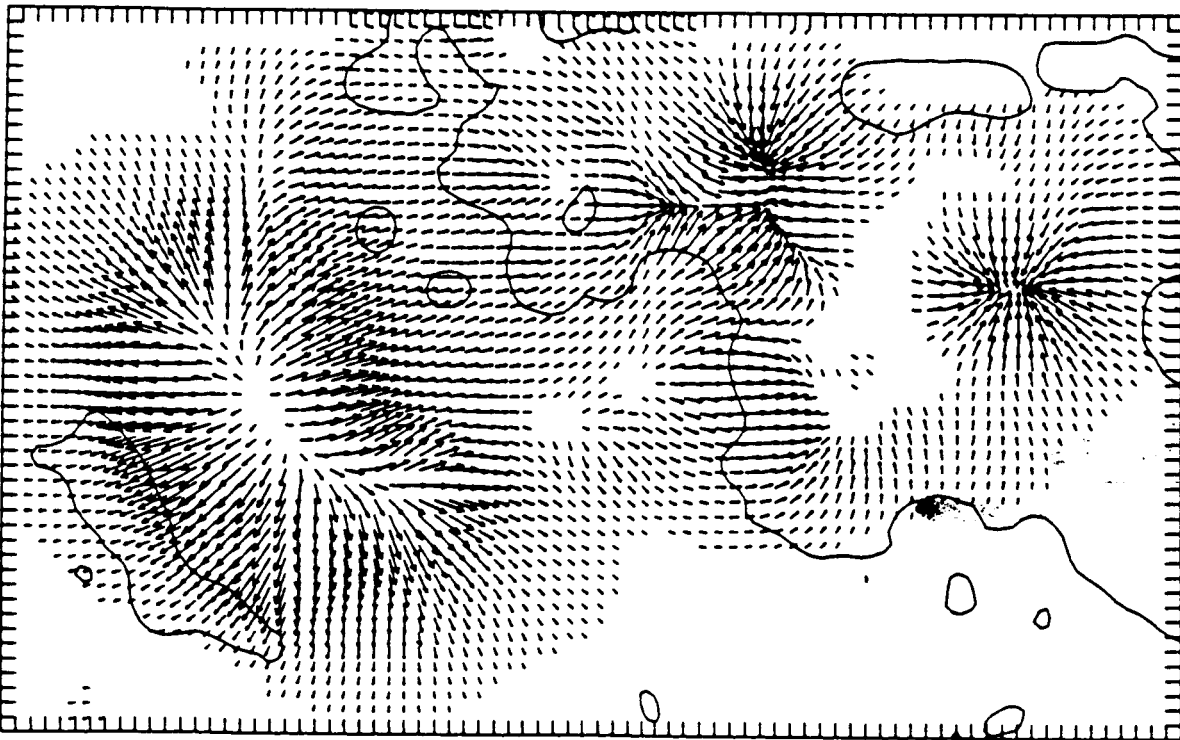
(a)



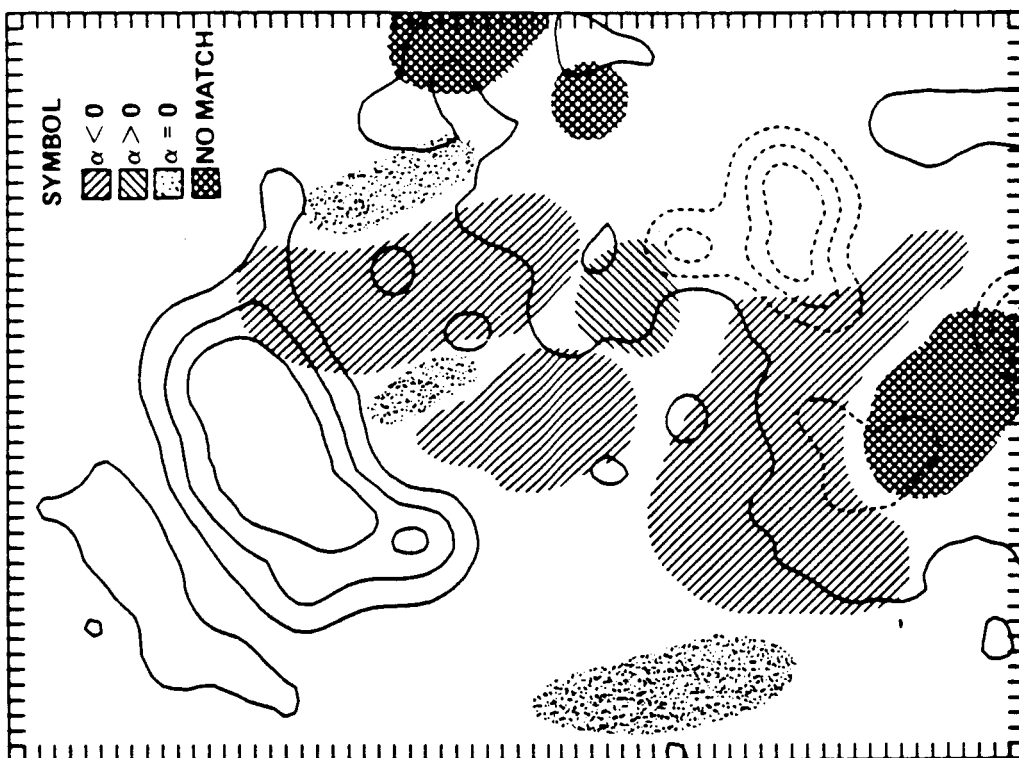
(b)



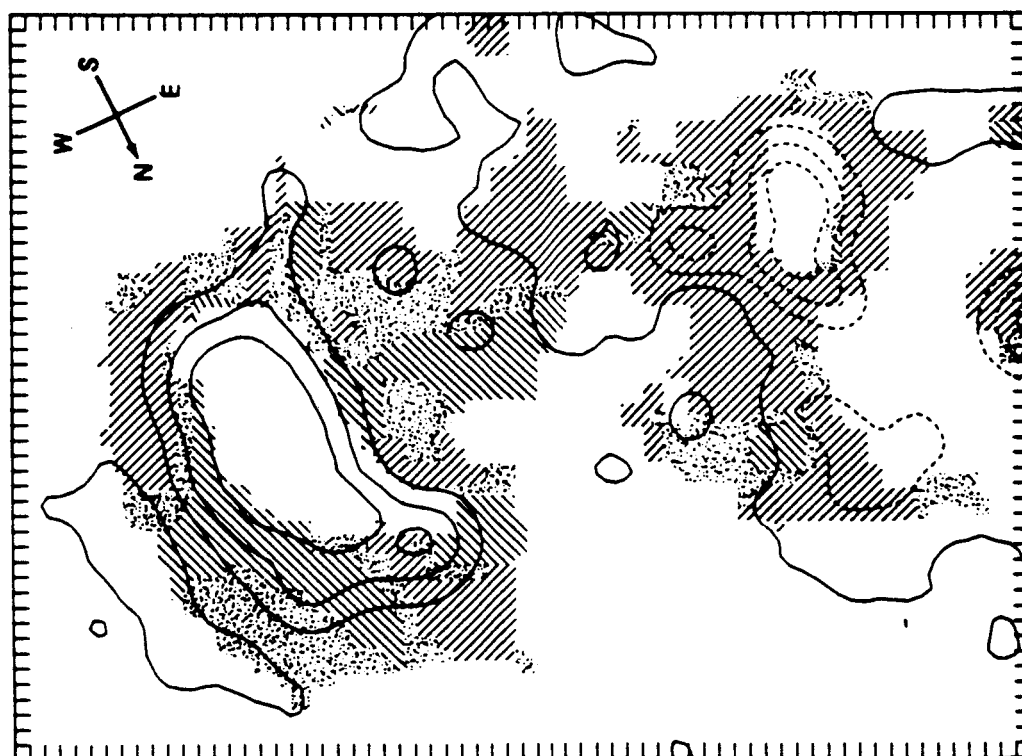
(b)



(a)



(b)



(a)